Three successive eruptions of a prominence observed by the coronagraph in NAO - Rozhen

Duchlev P., Koleva, K., Dechev, M., Petrov, N.
Institute of Astronomy and NAO, Bulgarian Academy of Sciences, 1784 Sofia, Tsarigradsko Chaussee blvd. 72
duchlev@astro.bas.bg
(Submitted on 25.06.2014. Accepted on 14.07.2014)

Abstract. A study of a rare event of three successive prominence eruptions observed with the $H\alpha$ coronagraph at the National Astronomical Observatory (NAO) – Rozhen is presented. The eruptive prominence is situated in active region NOAA 10904 and is associated with a narrow coronal mass ejection. The kinematics of the successive eruptions was analysed and compared. The obtained results suggest that the evolution of the eruptive prominence and the kinematic parameters of its successive eruptions are consistent with the so-called "homologous" eruptive events on the Sun.
Key words: solar eruptive prominences

1. Introduction

Solar prominences (or filaments, when observed on the disk) are formed and maintained above the magnetic polarity inversion line (PIL), in a magnetic structure called a filament channel, in which the filament can be supported by the magnetic field (see for review Martin, 1998). In terms of the magnetic environment of the PILs, there are three essential cases of prominence formation: **(i)** in weak magnetic fields at high latitudes (called polar crown prominences); **(ii)** in active regions (ARs), and **(iii)** at the borders of ARs or between two closely situated ARs (e.g. Leroy, 1989 for review). The final stage of a prominence is almost always an eruption (Filippov and Den, 2001) or in the case of a filament, the so-called "disparition brusque" (Raadu et al., 1987; Schmieder et al., 2000), when the filament faints away and disappears.

The relationship between eruptive prominences (EPs), large-scale eruptive phenomena such as CMEs and flares (Subramanian and Dere, 2001; Schrijver et al., 2008; Chandra et al., 2010; Yan et al., 2011), suggests that the three eruptive events occur in the same large-scale coronal magnetic field (e.g. Forbes, 2000; Li and Zhang, 2013). A three-part structure of a bright loop (helmet streamer), a dark cavity, and a prominence core often exists in the quiet corona (e.g., Gibson et al., 2006). The cavity is suggested to be the upper portion of a helical flux rope with cool filament material suspended at its bottom (e.g., Low 1996, 2001). CMEs exhibit an equivalent three-part structure: the bright core (EP), the dark cavity and the leading edge (e.g., Illing and Hundhausen, 1986). Thus, a detailed study of the origin and evolution of EPs is essential for a good understanding of their role in triggering CMEs (Schmieder et al., 2013), which will lead to a good ability to forecast CMEs and associated space weather.

Various studies indicate that prominences can erupt in many different ways depending on the prominence magnetic environment at all levels of the solar atmosphere and the physical processes occurring there (e.g. Joshi and Srivastava, 2011 for reviews). Solar prominences exhibit a range of eruptive behaviours, including a dramatic activation with the filament mass remaining confined to the low corona (e.g. Ji et al., 2003; Alexander et al., 2006; Török et al., 2010), the eruption of part of the observed filament structure (e.g. Zhou et al., 2006; Tripathi et al., 2013), and the almost complete eruption of all of the filament mass (e.g. Plunkett et al., 2000). A precise definition and a thorough discussion on the different types of eruption were made by Gilbert et al. (2007).

Prominence eruptions (full and partial) are often associated with coronal mass ejections (CMEs) and may play an important role in their initiation. The most common type of eruption is the partial eruption, where part of the prominence mass is observed falling back to the solar surface (see Gilbert et al., 2007). Partial eruptions are particularly interesting because of what happens after the eruptive part of the material escapes. The remaining supporting magnetic structure and prominence mass may relax or return to a lower altitude after the magnetic field reconfigures. Observationally, partial eruptions are most obvious on the limb, where parts of prominence material can be seen in the plane of the sky falling along apparent magnetic field lines (Gilbert et al., 2001). Occasionally these eruptions are also observed on the solar disk (Pevtsov, 2002; Liu et al., 2012).

EPs are often physically related to CMEs through common Magnetic Flux Ropes (MFRs) and the kinematic evolution of the EPs is very similar to the associated CMEs (Zhang et al., 2001). The EP kinematics typically shows three phases of evolution: an initiation (activation) phase, followed by a rapid acceleration, and a propagation. During the initial phase, the prominences (filaments) exhibit a slow rise during which both the filament and the overlying field expand with velocities in the range of 1–15 km s^{-1}. This is followed by a rapid acceleration phase during which velocities increase from 100 to over 1000 km s^{-1} (see for review Schrijver et al., 2008). Thereafter, the EP propagates with almost constant or slowly decreasing/increasing velocity depending on the interaction between its MFR and the ambient solar magnetic field. It is important to note that for the cases of partial and confined EPs there is another, last phase, during which the rest of mass of the partial EP and almost all the mass of confined EP is observed falling back to the solar surface (Gilbert et al., 2007).

In this article we analyze the kinematic evolution of a prominence that presents three successive eruptions on 2006 August 22. This EP is one of the rare cases of recurrent eruptions observed at the solar limb. We aim to compare the kinematic pattern of the different eruptions, as well as to clarify the relation between the EP and the associated narrow CME, the EP magnetic environment, and the associated radio events. The observations are described in Sect. 2. We present the kinematic patterns in Sect. 3. The analysis of the magnetic environment is given in Sect. 4. The associated radio events are presented in Sect. 5, the discussion and conclusions in Sect. 6 and the summary is given in Sect. 7.

2. Observations and Data Analysis

The EP was observed on 2006 August 22 at the National Astronomical Observatory – Rozhen with a 15 *cm* coronagraph through a $H\alpha$ 6563 Å filter (1.8

Å bandpass). The resolution of the $H\alpha$ filtergrams is $\sim 2''$. The images were obtained with a digital camera Canon EOS 350D (8 Mpxs). The first eruption was registered with an average cadence of 1.3 mins. The registered images, at maximal camera resolution, have a size of 3456×2304 px with a pixel size of 6.4×6.4 μm^2. The prominence height was determined as the height of the uppermost bright part of the prominence body above the limb in the radial direction.

We also used microwave images obtained with Nobeyama Radioheliograph (NoRH) at 17 GHz (Nakajima et al., 1994). NoRH is a radio telescope dedicated to observe the Sun. It consists of 84 parabolic antennas with 80 cm diameter and performs daily 8-hours full-disk observations. The spatial resolution at 17 GHz is $10''$. In our study we employ a time resolution of 10 minutes.

In this paper we present a set of observations performed at 164 MHz with the Nançay Radioheliograph (NRH). The NRH consists of 44 antennas with a size ranging from 2 to 10 m. The NRH observes the Sun approximatively seven hours per day in up to 10 frequencies between 150 and 450 MHz. The resolution of the 2 dimensional (2D) images depends on the frequency and on the season. The resolution range is approximately 3.2–5.5$'$(150 MHz) and 1.25–2.2$'$(432 MHz) (Kerdraon & Delouis, 1997).

3. Kinematic patterns

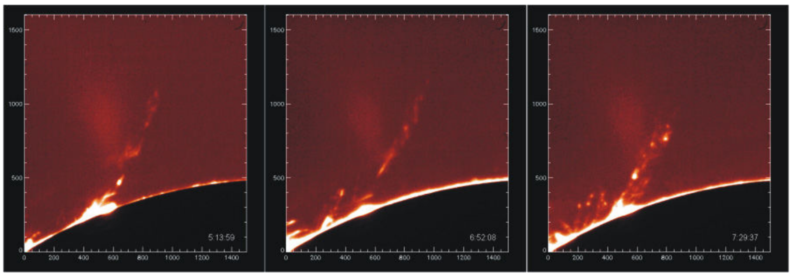

Fig. 1. NAO-Rozhen $H\alpha$ images of the EP on 22 August 2006 registered at the maximum height of the prominence for the first (left), second (center), and third eruptions (right).

The eruptive prominence was located in NOAA active region 10904. Its third eruption was associated with a narrow CME. The EP was observed on the southwestern quadrant of the limb at a location with a position angle (PA) of 250° (S20° W90°). The observations in the $H\alpha$ line were made between 04:47:55 and 07:31:44 UT during a time interval of 164 minutes. There also exist radio observations taken by the Nobeyama Radioheliograph at 17 GHz during a 120 minute time interval from 04:40 to 06:40 UT. The $H\alpha$ observations cover all three successive eruptions while the radio observations at 17 GHz recorded only the first prominence eruption and part of the second one.

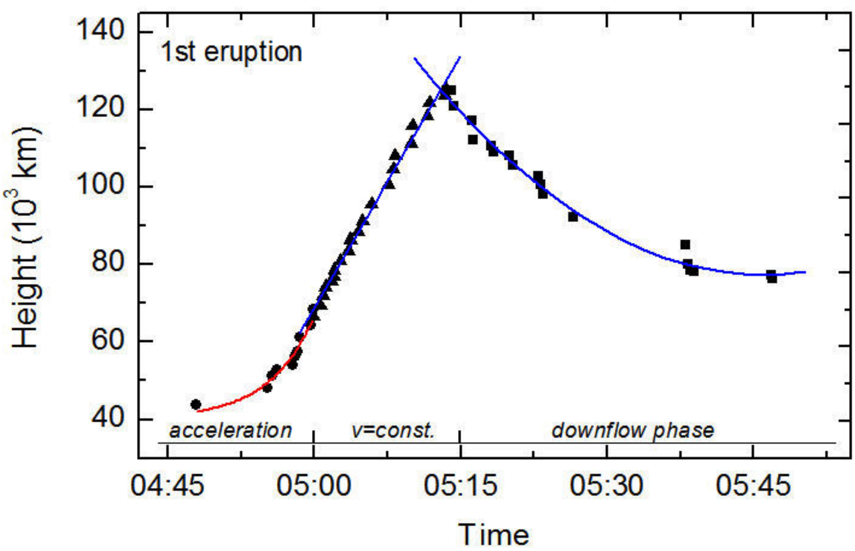

Fig. 2. Height-time profile of the first prominence eruption obtained from the $H\alpha$ observations.

The first prominence eruption lasted 59 minutes, from 04:47:55 to 05:46:57 UT, the second one 54 minutes, from 06:19:16 to 07:13:05 UT, and the third 13 minutes, from 07:18:51 to 07:31:44 UT. The three successive eruptions started at the same location at the solar limb (PA=250°). Each of them propagated upward in the corona under almost the same angle of $\approx 50°$ from the radial direction (see Fig. 1). Morphologically, the prominence body represents a magnetic flux rope build of helically twisted thin magnetic tubes filled with prominence plasma. During the first and second eruptions the EP body is tightly twisted, while during the third eruption, because of the untwisting motions and the increase of the MFR diameter, the thin treads that represent the magnetic flux tubes of the prominence body become well visible (Fig. 1).

The kinematic patterns of the three prominence eruptions are presented in Fig. 2, 3, and 4. The first eruption evolved through three stages (Fig. 2): (i) a rapid acceleration phase; (ii) a constant-velocity phase high in the corona; (iii) a downflow phase, when the prominence plasma flows back to the surface along the same trajectory. During the acceleration phase that lasted ~ 12 min (04:47:55 – 04:59:51 UT), the EP rapidly rose with an increasing velocity. The exponential fit for this phase gives the following kinematic values: the acceleration a increases from 27.6 to 104.4 m s^{-2}, the velocity v is from 28.5 to 111.4 km s^{-1}. The initial high values of a and v are due to a 7.3 min gap in the $H\alpha$ data between the first (04:47:55) and the second (04:55:12) measurement point. The constant velocity phase began at about 50 Mm above the solar surface and ended at maximum height of $\sim$150 Mm. It lasted $\sim$14 min (04:59:51 - 05:13:34 UT) with the EP rising with a velocity of 116.5 km s^{-1} estimated

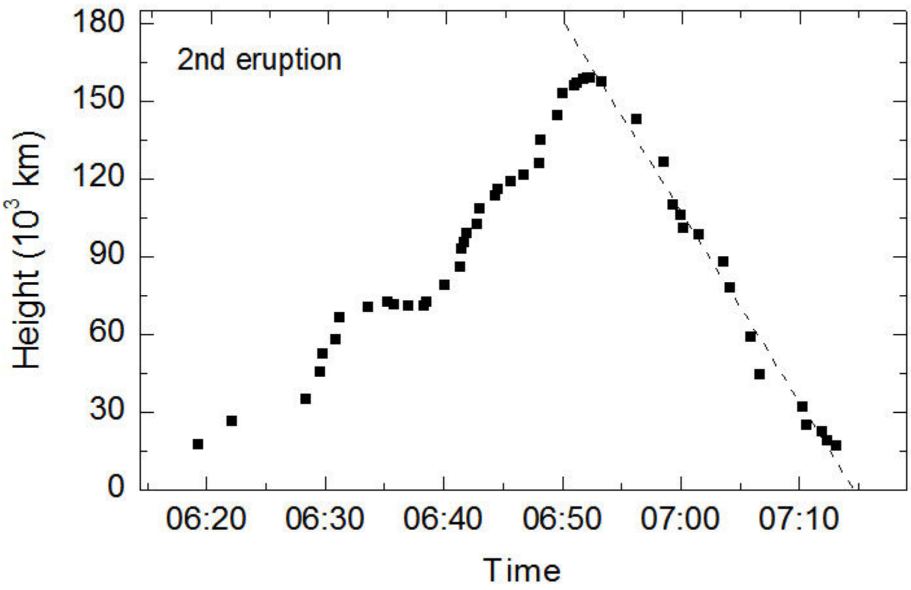

Fig. 3. Height-time profile of the second prominence eruption.

by a linear fit. The last, downflow phase, lasted 33.4 min, from 05:13:34 to 05:46:57 UT. A second-degree polynomial fit indicates that during this phase the prominence plasma drained back with a deceleration of 35.9 m s^{-2}. The velocity decreased from 118.2 km s^{-1} at height 145 Mm to 56.1 km s^{-1} at 75 Mm.

The second prominence eruption evolved through two stages (Fig. 3): (i) an eruptive phase and (ii) a downflow phase. The eruptive phase lasted ~33 min, from 06:19:16 to 06:51:50 UT, when the EP reached a maximum height of 159 Mm. This phase has certain peculiarities: it does not show the sequence of a typical prominence eruption, such as acceleration, constant velocity or slowly decreasing/increasing velocity. It rather exhibits a sequence of three similar behaviours, each consisting of an acceleration followed of a constant velocity stage. Because of this, the standard regression models are inapplicable to this phase. The downflow phase lasted ~21 min, from 06:52:08 to 07:13:05 UT. During the last phase, the prominence plasma flowed down with a velocity of 75 km s^{-1} estimated from a linear fit of the height-time profile.

The third prominence eruption lasted 13 min, from 07:18:51 UT to 07:31:44 UT. The prominence rose with a constant velocity of 26 km s^{-1}, and at 07:31:44 UT it reached a maximum height of 110 Mm. At the end of this eruption the prominence began to fade away in the Hα line and after 07:31:44 UT the EP MFR fully disappeared in the Hα line.

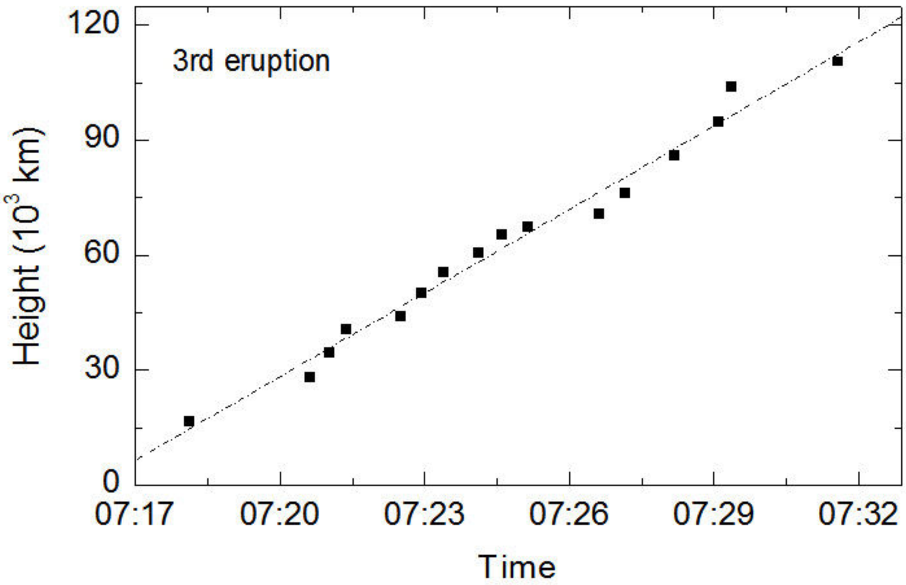

Fig. 4. Height-time profile of the third prominence eruption.

4. Magnetic Environment

The EP is associated with a filament in AR 10904 observed during the days prior to the region reach the solar limb. The filament was located in the immediate vicinity at the eastern side of the leading sunspot (Fig. 5) of the AR. The position of the EP at the limb suggests that the filament fragment located at 8° southward from the AR center erupted on 22 August 2006. The leading sunspot of AR 10904 became first clearly visible at the east limb on August 11 when the AR had a class $\beta\gamma/\alpha$ according to the Hale classification (Hale & Nicholson, 1938). In total 23 soft X-ray (SXR) flares of class C occurred in the AR during its existence. The filament became clearly visible on 16 August 2006. Its evolution can be traced on the Hα filtergrams in Fig. 5. On August 20 the filament was almost ring shaped encircling the area of the positive magnetic flux in AR 10904. This is well seen on the synoptic chart of the photospheric magnetic field from the Wilcox Solar Observatory (Fig. 6). The AR was in a decaying phase of α/β Hale class, when the filament eruption occurred. The characteristics of the AR 10904 for the six days until the eruption are presented in Table 1.

The LASCO C2 coronagraph observed four CMEs associated with AR 10904 and one of them is linked to the eruptive prominence/filament (Fig. 7). The CME traveled along a coronal streamer with a PA of 239° and an angular width of only 14°, i.e. it represents a narrow CME. The CME first appears in the LASCO C2 field-of-view (FOV) at 09:12:04 UT. Its start time estimated by the linear approximation of the CME propagation is 06:55:12 UT, the time

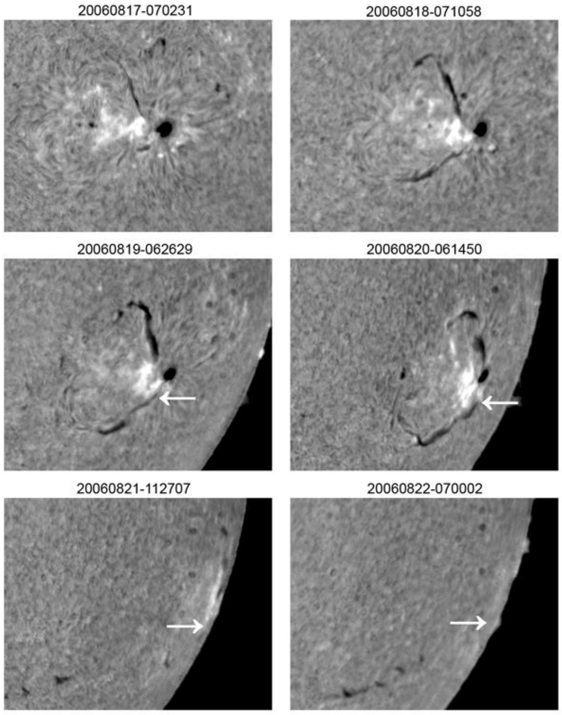

Fig. 5. Series of Hα images from the Kanzelhöhe Solar Observatory showing the evolution of the filament located in the NOAA AR 10904. White arrows point at the filament part producing the eruptions.

when the second prominence eruption reached a maximum height. The linear CME speed is 234 km s^{-1} and the second-order speed is 163 km s^{-1} with a deceleration of $-24.3\ m\ s^{-2}$. It is important to note that other three CMEs appeared almost every hour just before the start time (04:47:55 UT) of the first prominence eruption. The physical parameters of the CMEs according to the LASCO CME catalog are given in Table 2.

The EP propagation during the three successive eruptions shows a deflection of about $\approx 50°$ from the radial direction through its starting point at the solar limb. In a composite LASCO C2 and solar grid image (Fig. 7) one can see that the EP is located in the northern outer flank of the coronal streamer base. In the inner corona the filament eruption underwent non-radial motion, while the CME had a radial path along the streamer that was laterally offset from the original site of the filament. Recently, Jiang et al. (2009) presented observations of a streamer-puff CME that resulted from a spectacular eruption of an active-region filament inside a single helmet streamer consisting of a double-arcade system occurring in AR 10792 on 2005 July 29. Such observations can be explained by the magnetic-arch-blowout scenario for streamer-puff

Table 1. Active region NOAA 10904

Date	Location	Hale Class	Area	Flare Events
20060617	S12W29	$\beta\gamma/\beta\gamma$	0600/0700	C1.0(04:27) C3.6(14:37) C3.5(18:44)
20060618	S13W42	$\beta\gamma/\beta\gamma$	0590/0600	C1.0(04:27)
20060619	S13W56	$\beta\gamma/\beta\gamma$	0590/0590	
20060620	S14W68	$\beta\gamma/\beta\gamma$	0540/0590	C1.6(11:55) C2.9(16:27) C4.3(21:02) C3.8(11:16) C2.2(21:13)
20060621	S14W86	β/β	0520/0540	C4.7(19:07) C2.9(16:27) C4.3(21:02)
20060622	S12W91	α/β	0180/0520	C4.7(19:07)

Table 2. The CMEs parameters according to LASCO CME catalog

First C2 Appearance Date	Time [UT]	MPA * [deg]	Angular Width [deg]	Linear Speed [km/s]	2^{nd}-order speed at final height [km/s]	Accel. [m/s2]
2006/08/22	01:36:05	237	9	337	364	10.7
2006/08/22	02:24:04	238	16	339	311	-4.0
2006/08/22	04:00:04	244	11	361	444	4.5
2006/08/22 1	09:12:04	239	14	234	163	-24.3

*Measurement Position Angle - the position angle at which the height-time measurements are made

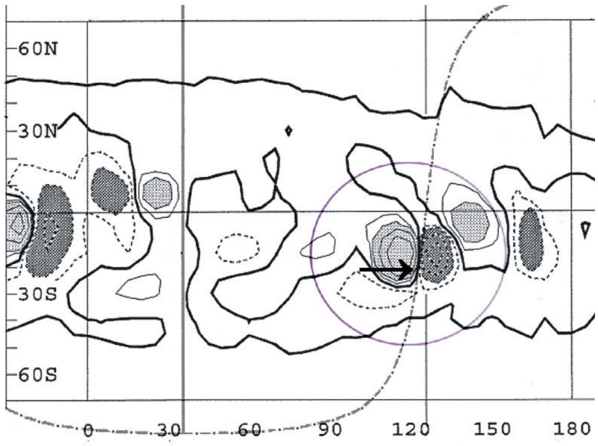

Fig. 6. Part of a photospheric magnetic field synoptic chart of the Wilcox Solar Observatory for Carrington rotation 2046, showing the magnetic field in NOAA AR 10904. The solar limb is overplotted with dashed-dotted line. The arrow points at the eruption position.

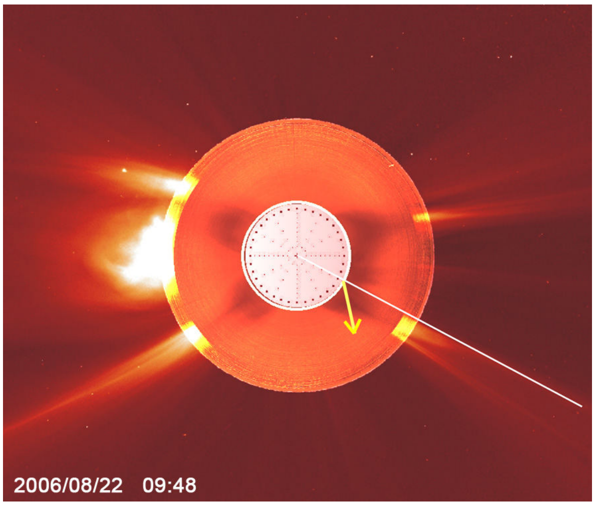

Fig. 7. Composite image of the LASCO C2 with over-imposed solar grid. The white line indicates the radial direction through the prominence eruption location. The yellow arrow indicates the non-radial direction of the eruption.

and over-and-out CMEs, in which the streamer arcade can act on the erupting filament, laterally deflecting and channeling its motion (Jiang et al., 2009).

5. Radio Events

The prominence eruption event on 22 August 2006 was also observed by the Nobeyama Radioheliograph (NoRH) at 17 GHz between 04:40 and 06:40 UT. Hence, the NoRH microwave observations cover the whole first eruption of the prominence and part of second one (Fig. 8). The early stages of the eruptions are not clearly visible because the AR is a strong source of microwave emission at 17 GHz and obstructs them. However, the late stages of the prominence eruptions are well seen and they distinctly exhibit the apparent non-radial direction of the eruptions. The kinematics of the eruptions, especially the first one, is similar to those determined from the Hα images. There are some differences between the prominence evolution observed in Hα and 17 GHz, which are related to a number of characteristics such as shape, morphology, and brightness temperature.

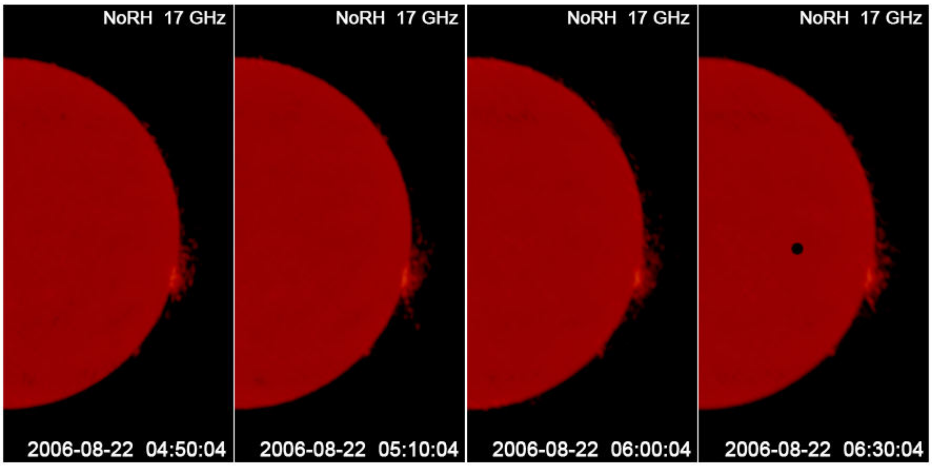

Fig. 8. Nobeyama Radioheliograph 17 GHz images of the EP on 22 August 2006. The left two images show the EP in the beginning of the first eruption at its maximum height. The right two images present the beginning of the second eruption at almost its maximum height.

Fig. 9 presents a sample of two radio observations of the Sun at 164 MHz, made by the Nançay Radioheliograph (NRH). The radio observations at 164 MHz were made between 08:42:38 and 09:24:13 UT. The dominant source of the continuum measured by the NRH at distinct frequency is located above the limb (at PA=237°) southwards from the EP limb position (Fig. 9). It is important to note that the limb arc, located between the radio source and the EP (Fig. 9), is the position where the CMEs appeared (Table 2). The radio source drifts outwards, changing its altitude nearly from 1.3 (08:42:38 UT) to 1.85 (09:10:22 UT) solar radii, then it began to fade away until its full disappearance at 09:24:13 UT.

The drifting of the intense outburst at 164 MHz from the low to the high corona suggests type III bursts. This is supported by the WIND/WAVES

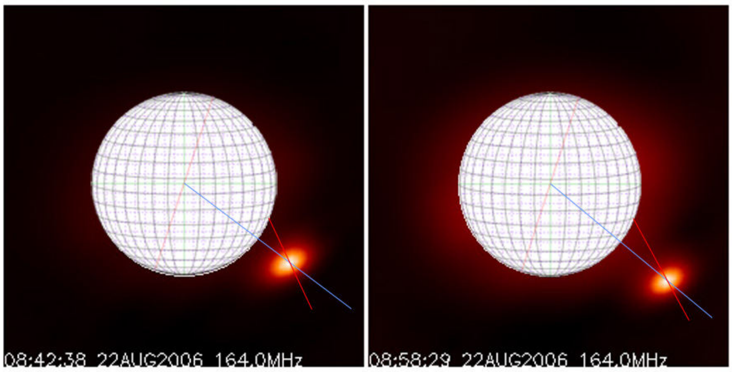

Fig. 9. Composite images of Nançay Radioheliograph images at a frequency of 164 MHz with the over-imposed solar grid. The picture presents the first (left) and late (right) registrations of the 164 MHZ radio burst. The blue line indicates the radial direction through the center of 164 MHz outburst. The red line indicates the direction from the eruption position at the limb to the outburst center.

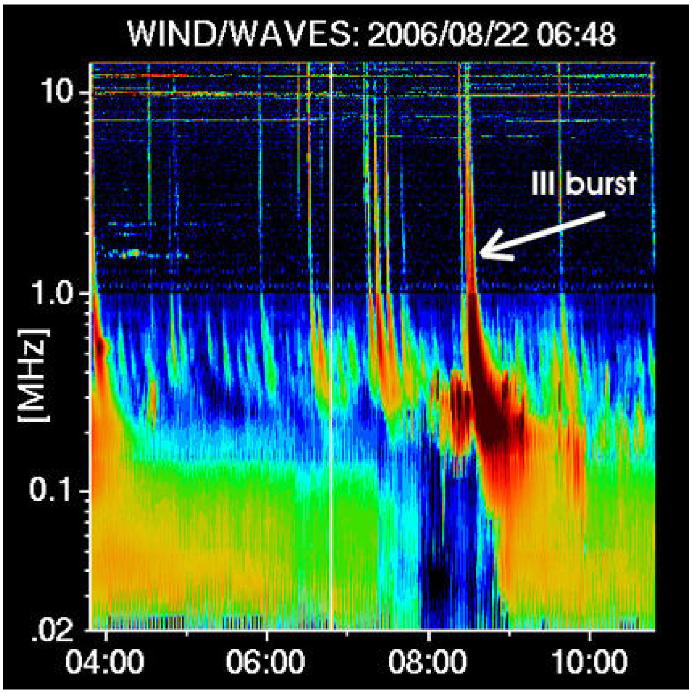

Fig. 10. WIND/WAVES dynamic spectrum between 03:48 UT and 10:48 UT on 22 August 2006.

dynamic spectrum shown in Fig. 10. The spectrum period covers the three prominence eruptions, the 164 MHz radio source evolution, and the associated CME event. The III-type radio burst registered in the dynamic spectrum is co-temporal with the NRH 164 MHz event.

6. Discussion and Conclusions

We studied three successive eruptions of a solar filament formed in AR 10904 and observed with the Hα coronagraph at NAO-Rozhen as prominence eruptions on the solar limb. The durations of the first and second eruptions are roughly equal, close to an hour. The duration of the third eruption is under question as the prominence faded and disappeared in the Hα line after 13 min of eruption. The kinematic profiles of the first and second eruptions are similar. They exhibit two basic stages, eruptive and post-eruptive (downflow) ones. The eruptions were followed by plasma returning back to the chromosphere suggesting a confined (failed) eruption. The second eruption has two special features, a specific kinematic behaviour of the eruptive phase, which represents a sequence of three "acceleration-constant velocity" subphases and a maximum height bigger than those of the first eruption. The third (final) eruption is associated with a narrow CME. There is no detailed information on this eruption because the prominence disappeared in Hα early in its eruption, therefore, we can not define with certainty whether it is a partial or full type eruption. However, the radio observations at 164 MHz indicate a possible full eruption.

An essential feature of the prominence eruptions is the same non-radial direction of their propagations, at an angle of about 50° to the radial direction. The non-radial motion of an erupting filament near the surface in association with a radial CME in the outer corona is rarely reported (e.g. Jiang et al., 2009). In this context, our event is one of the rare cases registered by ground-based coronagraph observations.

The structure of the magnetic field around the filament and its evolution are crucially important in triggering and driving successive eruptions (e.g. Zou et al., 2006; Jiang et al., 2009), as well as in determining the direction of these eruptions (e.g. Filippov & Gopalswamy, 2001; Filippov, 2013). The MFR of the EP of 22 August 2006 is located beneath the northern flank of a coronal streamer and is offset in heliolgraphic latitude from the centers of the streamer and the associated CME. The CME is asymmetrically located with respect to the bipolar magnetic field system of AR 10904 (Fig. 7). We should note that such magnetic complexities are no rare events. Filament eruptions tend to be systematically offset in latitude from the centre of their associated CMEs (e.g. Gopalswamy et al., 2003). Hence, our event is consistent with eruptions in the presence of multiple arcades, for which the interplay or interaction between different magnetic arcades is fundamental for the eruption process (Jiang et al., 2009). Our results for non-radial motions of the EP are consistent with the model of Filippov & Gopalswamy (2001), which shows that a streamer can exert an effect on a filament and so guide its eruption. The non-radial ejection reported here also agrees with recent observations showing that erupting filaments can be deflected by another magnetic structure (Jiang et al. 2007, 2009).

The three successive prominence eruptions start from the same place on the solar limb, i.e. from the same region within AR 10904. The eruptions have a similar coronagraph appearance and, generally, similar morphology, which suggests that the endpoints of their MFRs are anchored in the same region. Therefore, these eruptions are consistent with the criteria for so called "homologous" eruptive events (flares, EPs, CMEs) defined by Li & Zhang (2013).

The third prominence eruption is observed in Hα for almost 13 min. Its duration in comparison with the eruptive phases of the previous two eruptions (26 and 33 min) suggests that the eruptive phase duration is of the order of the previous two ones. Thus, for the entire third eruption a duration of about an hour can be estimated. Approximately an hour after the third eruption onset, the first intense outburst at 164 MHz was observed. According to the WIND/ WAVES dynamic spectrum (Fig. 10), it represents a III-type burst. The slow outward drifting of the radio burst lasts until 09:12:04 UT, when the CME becomes visible in the LASCO C2 FOV. Radio emission is the signature of the magnetic field restructuring at the edges of CMEs. Observations of type III bursts provide strong support for the production of non-thermal electron beams in the cusp reconnection sites (Pick & Vilmer, 2008). In reconnection models (e.g. Kopp & Pneuman, 1976), an initial, close and stressed magnetic configuration becomes unstable and erupts. Magnetic field lines are then stretched by the eruption and a current sheet is formed above the photospheric magnetic inversion line, behind the erupted flux rope. Magnetic reconnection occurs along this current sheet, first at low altitude, then at progressively higher ones (see Forbes, 1996). The topology and the evolution of the emitting sources strongly suggests successive interactions between rising arches and other loops. The electrons responsible for the flux enhancements could be the result of these magnetic interactions (Pick et al., 1998).

7. Summary

Our main results can be summarized as follows.

1. Our observations present a rare event that exhibit three successive prominence eruptions at the solar limb. The kinematic patterns of the first two eruptions are similar exhibiting an eruptive phase and a downflow phase. The differences between them are the bigger maximum height of the second eruption and the peculiarity of its eruptive phase behaviour. The third eruption is successful (partial or full), but its kinematic pattern is not full because of the early disappearance of the prominence in Hα.

2. The EP presents successive eruptions of a fragment of a filament located in AR 10904. The MFR of the EP is located beneath the northern flank of a coronal streamer and is associated with a narrow CME that propagates in an asymmetric position with respect to the AR. The presence of multiple arcades and their interplay or interaction are the most probable reason for the non-radial direction of the prominence eruptions, at an angle of $\approx 50°$ to the radial direction.

3. The type III burst observed at 164 MHz that slow drifts outward could be considered as a radio signature of the reorganization of the overlaying magnetic arcade resulting in the magnetic field restructuring at the edges of the associated CME (e.g. Pick et al., 2005).

4. The similar coronagraph appearance of the three prominence eruptions, their start from the same location on the solar limb, i.e. from the same region within AR 10904, and the same non-radial direction of the eruptions strongly suggests that the EP on 22 August 2006 presents a triple homologous eruption.

Acknowledgements

We are grateful to the instrumental teams of the NoRH and NRH for their open-data policies. Hα data were provided by the Kanzelhöhe Observatory, University of Graz, Austria. The SOHO/LASCO data used here are produced by a consortium of the Naval Research Laboratory (USA), Max-Planck-Institut fuer Aeronomie (Germany), Laboratoire d'Astronomie (France), and the University of Birmingham (UK). SOHO is a project of international cooperation between ESA and NASA. The WIND/WAVES instrument is a joint effort of the Paris-Meudon Observatory, the University of Minnesota, and the Goddard Space Flight Center.

References

Alexander, D., Liu, R., Gilbert, H. R., 2006, *ApJ* **653**, 719
Chandra, R., Pariat, E., Schmieder, B., Mandrini, C. H., Uddin, W., 2010, *Solar Phys.* **261**, 127
Filippov, B. P., 2013, *ApJ* **773**, 10
Filippov, B. P., Den, O. G., 2001, *J. Geophys. Res.* **106**, 25177
Filippov, B. P., Gopalswamy, N., 2001, *Solar Phys.* **203**, 199
Forbes T. G., 1996, *Am. Inst. Phys. Conf. Ser.* **374**, 275.
Forbes, T. G., 2000, *J. Geophys. Res.* **105**, 23153
Gibson, S. E., Foster, D., Burkepile, J., de Toma, G., Stanger, A., 2006, *ApJ* **641**, 590
Gilbert, H. R., Holzer, T. E., Burkepile, J. T., 2001,*ApJ* **549**, 1221
Gilbert, H. R., Alexander, D., Liu, R., 2007, *Solar Phys.* **245**, 287
Gopalswamy, N., Shimojo, M., Lu, W., Yashiro, S., Shibasaki, K., Howard, R. A., 2003, *ApJ* **586**, 562
Hale, G. E. , Nicholson, S. B., 1938,*Magnetic observations of sunspots 1917–1924*, Washington, D.C. Carnegie Institution of Washington
Illing, R. M. E., Hundhausen, A. J., 1986, *J. Geophys. Res.* **91**, 1095
Jiang, Y., Yang, L., Li, K., Shen, Y., 2007, *ApJ* **667**, L105
Jiang, Y., Yang, J., Zheng, R., Bi, Y., Yang, X., 2009, *ApJ* **693**, 1851
Joshi, A. D., Srivastava, N., 2011, *ApJ* **730**, 104
Kerdraon, A., Delouis, J., 1997, *Coronal Physics from Radio and Space Observations*; Proceedings of the CESRA Workshop held in Nouan le Fuzelier, France 3-7 June 1996, edited by Gerard Trottet, Published by Springer, 192
Kopp, R. A., and Pneuman, G. W., 1976, *Solar Phys.* **50**, 85
Leroy, J.-L., 1989, in *Dynamics and Structure of Quiescent Solar Prominences*, E. R. Priest (ed.), 77
Li, T., Zhang, J., 2013, *ApJ* **778**, L29
Liu, W., Ofman, L., Nitta, N. V., et al., 2012, *ApJ* **753**, 52
Low, B. C., 1996, *Solar Phys.* **167**, 217
Low, B. C., 2001, *J. Geophys. Res.* **106**, 25141
Martin, S. F., 1998, *Solar Phys.* **182**, 107
Nakajima, H., Nishio, M., Enome, S., and 14 coauthors, 1994, *Proc. IEEE*, Vol. **82**, No. 5, 705
Pevtsov, A. A., 2002, *Solar Phys.* **207**, 111
Pick, M., Vilmer, N., 2008, *A&ARv* **16**, 1
Pick M, Malherbe J-M, Kerdraon A, Maia D.J.F., 2005, *ApJ* **631**, L97
Pick, M., Maia, D., Kerdraon, A., and 10 coauthors, 1998, *Solar Phys.* **181**, 455

Plunkett, S. P., Vourlidas, A., Šimberová, S., Karlický, M., Kotrč, P., Heinzel, P., Kupryakov, Yu. A., Guo, W. P., Wu, S. T., 2000, *Solar Phys.* **194**, 371
Raadu, M. A., Malherbe, J. M., Schmieder, B., Mein, P., 1987, *Solar Phys.* **109**, 59
Schmieder, B., Delannée, C., Yong, D. Y., Vial, J. C., Madjarska, M., 2000, *A&A* **358**, 728
Schmieder, B., Démoulin, P., Aulanier, G., 2012, *AdvSpR* **51**, 1967
Schrijver, C. J., Elmore, C., Kliem, B., Török, T., Title, A. M., 2008, *ApJ* **674**, 586
Subramanian, P., Dere, K. P., 2001, *ApJ* **561**, 372
Török, T., Berger, M. A., Kliem, B., 2010, *A&A* **516**, A49
Tripathi, D., Reeves, K. K., Gibson, S. E., Srivastava, A., Joshi, N. C., 2013, *ApJ* **778**, 142
Yan, X. L., Qu, Z. Q., Kong, D. F., 2011, *MNRAS* **414**, 2803
Zhang, J., Dere, K. P., Howard, R. A., Kundu, M. R., White, S. M., 2001, *ApJ* **559**, 452
Zhou, G. P., Wang, J. X., Zhang, J., et al., 2006, *ApJ* **651**, 1238